Ground deformation at Mt. Etna: a joint interpretation of GPS and InSAR data from 1993 to 2000

M. Palano[1], G. Puglisi[1] and S. Gresta[2]

[1] *Istituto Nazionale di Geofisica e Vulcanologia, Sezione di Catania, Italy*
[2] *Dipartimento di Scienze Geologiche, Università degli Studi di Catania, Italy*

(Received March 9, 2006; Accepted November 11, 2006)

ABSTRACT Combined Global Positioning System (GPS) measurements and Interferometry SAR (InSAR) have been applied on Mt. Etna to study the ground deformation affecting the volcano both over the long (1993-2000) and short-term (1997-2000). From 1993 to 1997, data indicate a re-pressurization of Mt. Etna's plumbing system that i) triggered most of the seismicity, ii) induced the dilatation of the volcano, and iii) produced a series of summit eruptions since 1995. InSAR detected a deep intrusion on the western flank of the volcano, between March and May 1997. In the following months, this intrusion rose leading to a seismic swarm in the western sector occurring in January 1998. The shallow intrusion is confirmed by GPS data. From 1998 to 2000, a general deflation affected the upper part of the volcano. Elastic deformation modelling of GPS data suggests that the active sources of deformation include deep pressure sources located beneath the upper western flank of the volcano, shallow dislocation sources (dikes and faults) located beneath the NE and S rift zones, and a sub-horizontal dislocation plane (dipping about 12° ESE), located beneath the eastern flank of the volcano at a depth of 1.5 km b.s.l.. InSAR data validated these models.

1. Introduction

On an active volcano, the intrusion of magma bodies or the emptying of magma reservoirs produce ground deformations. Several authors have observed measurable ground deformation since the early experience reported by Omori (1914), who deduced it from the changing heights of benchmarks accompanying the 1914 eruption of Sakurajima volcano in Japan. Techniques for monitoring ground deformation have been greatly improved in recent years and at present active volcanoes are monitored not only by using terrestrial techniques (e.g. precise levelling and trilateration) but also from space, thanks to the availability of techniques such as the Global Positioning System (GPS) and the Synthetic Aperture Radar Interferometry (InSAR).

Although GPS is the most suitable technique for measuring ground deformation, it provides spot data, i.e. they refer to network vertices whose number rarely exceeds the order of tens in areas of hundreds, often thousands of square kilometres. InSAR continuously measures the range between the Earth's surface and the sensor along the Line Of Sight (LOS) across the investigated area (i.e. it has a scalar dimension). Its introduction has been seen as the only way of having a continuous map of gradients of ground deformation patterns, although with a lower absolute accuracy than the GPS. Even if both InSAR and GPS provide measurements of the ground deformation pattern, they do have several differences, such as the accuracy, the kind of data (mono-dimensional for SAR and three-dimensional for GPS), the number of samples of ground deformation patterns (very large for InSAR

with respect to GPS) or the extension of investigated areas (usually larger for InSAR with respect to GPS).

Therefore, the joint use of InSAR and GPS is a powerful tool to study the ground deformation pattern over large areas such as a volcano like Mt. Etna: the accuracy of GPS data allows the validation of InSAR data, while InSAR data allows us to obtain continuous maps of the gradients of ground deformation patterns across the benchmarks of a GPS network. Hence, an approach that integrates InSAR-GPS results has the potential to detect highly accurate deformations (i.e. at sub-centimetre levels) with unprecedented spatial coverage.

The aim of this paper is to use the integrated InSAR-GPS approach in order to constrain both long and short-term ground deformation patterns affecting Mt. Etna volcano during 1993-2000.

2. Tectonic setting

Mt. Etna is a large Quaternary polygenetic volcano, 3340 m high, located on the eastern coast of Sicily (Fig. 1).

The volcanic edifice is characterised by a geodynamical setting resulting from complex regional tectonics with a compressive stress regime, active in northern Sicily along an approximate N-S trend and an extensional regime roughly trending E-W, observable along the eastern coast of Sicily [see Bousquet and Lanzafame (2004) for an overall review]. The eastern flank of the volcano edifice shows a continuous eastward movement. Many authors have argued that the eastern flank of the volcano is affected by an ESE seaward sliding due to the interrelationship between gravity instability and magma intrusion (e.g., Borgia *et al.,* 1992; Lo Giudice and Rasà, 1992; Rust and Neri, 1996; Bonforte and Puglisi, 2003). Although these authors propose different models to explain the origin of this flank movement, they all agree on identifying the Pernicana fault system (Fig. 1) as the northern boundary of the unstable sector. This fault system is formed by discrete segments, arranged in a right-stepping *en échelon* configuration, of a near continuous left-lateral shear zone that dissects the NE flank of Mt. Etna. Westwards, the fault joins with the NE Rift, which represents one of the most active volcanic features (Fig. 1). The southern boundary of the unstable sector is represented by the S Rift (Rasà *et al.,* 1996) joining, south-eastwards, with the Mascalucia-Tremestieri-Trecastagni fault system (Fig. 1). This fault system is made up of a number of NNW-SSE-striking faults showing evident right lateral displacement and is also characterised by very shallow seismicity, with focal depths typically of 1-2 km. However, other authors identify the Ragalna fault (Fig. 1) as the south-western boundary of the sliding sector (Borgia *et al.,* 1992; Rust and Neri, 1996). The Ragalna fault displays a consistent pattern of right-oblique displacement of cultural features as well as open left-stepping e*n échelon* fissures. Focal mechanism solutions of local shallow earthquakes show a right-lateral slip (Azzaro, 1999). The activity of this fault system has also been recently highlighted by InSAR data (Froger *et al.,* 2001; Lundgren *et al.,* 2004).

Several other faults dissect the eastern sector of the volcano (Fig. 1), all recognized by significant shallow seismicity ($h < 5$ km) and/or creep phenomena (Gresta *et al.,* 1997).

3. Mt. Etna's activity from 1993 to 2000

After the 1991-93 eruption, a period of low volcanic activity (Fig. 2a), characterized by a

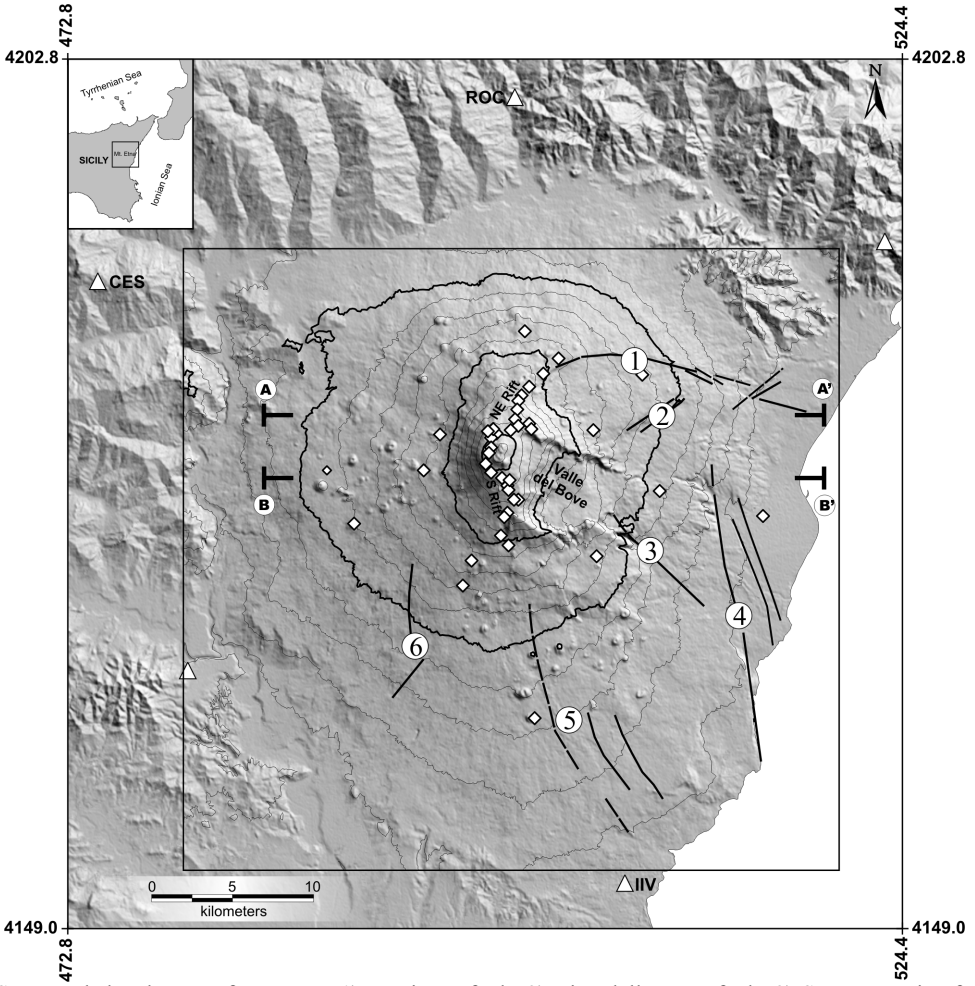

Fig. 1 - Structural sketch map of Mt. Etna: 1) Pernicana fault; 2) Ripe della Naca fault; 3) Santa Venerina fault; 4) Timpe fault system and Moscarello fault; 5) Mascalucia-Tremestieri-Trecastagni faults system, 6) Ragalna fault. Mt. Etna GPS Network is also reported: diamond for inner benchmarks, triangle for external reference benchmarks. Coordinates in UTM projection, zone 33N. The box indicates the area shown in Figs 3, 4, 5, 6 and 7. A-A' and B-B are schematic cross-sections reported in Fig 7.

continuous degassing interrupted only by a few phreatic explosions, began at the summit vents (Coltelli *et al.,* 1998).

Magmatic activity resumed in July 1995, at the Bocca Nuova crater (BNC), then spread to the NE crater (NEC) in early August (Coltelli *et al.,* 1998). From November 1995 to August 1996, the NEC was the site of spectacular explosive and effusive activity including ten episodes of lava fountaining, while BNC had mild Strombolian explosions and small lava overflows (Coltelli *et al.,* 1998).

In early November 1996, Strombolian activity resumed at the SE crater (SEC). In June 1997, the eruptive activity of the SEC increased so that lava flows spilled eastwards over the crater rim. In summer 1997, Voragine (VOR), which had been actively degassing from a pit in its floor since

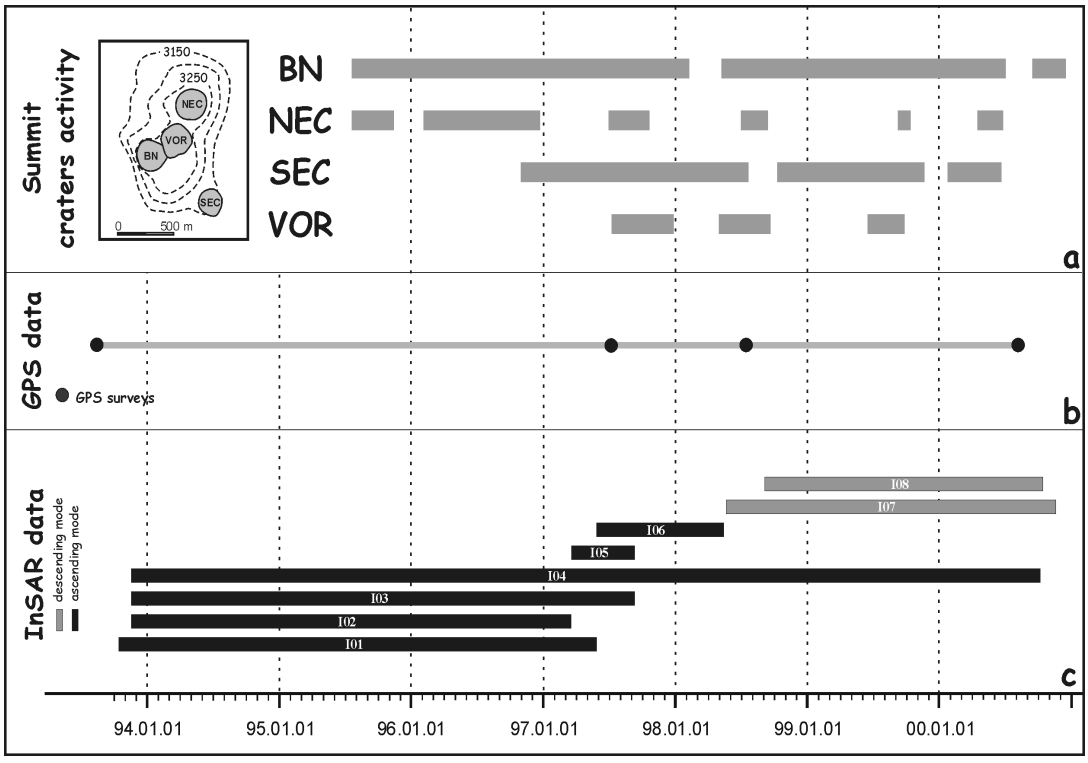

Fig. 2 - a) Graphic illustration of the activity at the summit craters during 1993-2000 (BN, Bocca Nuova; NEC NE Crater; SEC, SE Crater; VOR, Voragine); b) time coverage for the GPS data; c) time coverage for InSAR data.

1991, resumed discontinuous Strombolian activity (Rothery *et al.,* 2001).

In January 1998, a seismic swarm (M_{max} = 3.7) marked a shallow dike intrusion below the summit area (Bonaccorso and Patanè, 2001). In the following months, the increase in eruptive activity was marked by strong explosive activity, first at the NEC in March and afterwards at VOR in June. Lava flows from SEC continued until July 1998, when a further paroxysmal eruptive episode was produced by VOR (Fig. 2a). Simultaneously, strong activity occurred at BNC and SEC also (Rothery *et al.,* 2001).

On September 15, 1998, activity resumed at SEC with a lava fountain. It was the first of 21 lava fountain episodes at SEC. The last episode (February 4, 1999) was particularly important because a new eruptive fissure opened at the base of SEC, allowing lava to effuse quietly beyond the crater for the next 9 months (Rothery *et al.,* 2001). The other summit vents were inactive until July 1999, when VOR resumed Strombolian activity culminating in a paroxysmal explosive episode on September 4. Then, eruptive activity became strong and continuous, producing Strombolian explosions and lava fountains from both SEC and BNC (Fig. 2a).

Activity at BNC resumed in October 1999, with near-continuous lava fountaining. In January 2000, the SEC reawakened with violent lava fountaining and production of lava flows. Its cone split open on its southern side. The activity at SEC ceased at the end of August 2000. From

Table 1 - Code, UTM coordinates, height and measurements for each benchmark of the Mt. Etna GPS Network (see also Fig. 1). Static and kinematic are relevant to the techniques used to survey GPS benchmarks. In general, the time occupation for static mode ranges from 4 (inner benchmarks) to 8 hours (external reference benchmarks), with a sampling rate of 30 s. The time occupation for the kinematic mode is about 4 minutes, with a sampling rate of 5 s. In the kinematic mode, each benchmark is surveyed twice during the same session (fore and back) allowing a good compromise between density of measured points and accuracy [more details in Puglisi and Guglielmino (1995)].

CODE	LONG.	LAT.	HEIGTH	1993	1997	1998	2000	survey mode
CAP	494784	4177299	1922		♦	♦	♦	static
CAS	523288	4191439	842		♦	♦	♦	stati
CES	474742	4188986	1247	♦	♦	♦	♦	stati
CIS	500633	4175479	2682		♦	♦	♦	static
CIT	505241	4179808	1781	♦	♦	♦	♦	static
CRI	508250	4183202	1384	♦	♦	♦	♦	static
CRP	480290	4164967	339	♦	♦	♦	♦	static
EPLU	498743	4179753	2964			♦	♦	static
ESLN	497776	4171760	1774	♦	♦	♦	♦	static
GIA	515722	4174501	164		♦	♦	♦	static
IIV	507253	4151853	88	♦	♦	♦	♦	static
L23	503092	4184205	1955	♦	♦	♦	♦	static
LAM	501013	4185857	1751	♦	♦	♦	♦	static
MIL	509308	4176052	921	♦	♦	♦	♦	static
MPL	501671	4162063	795		♦	♦	♦	static
NS01	502150	4183270	2134		♦	♦	♦	kinematic
NS02	501282	4182457	2357		♦	♦	♦	kinematic
NS03	500859	4181959	2456		♦	♦	♦	kinematic
NS04	500616	4181603	2538		♦	♦	♦	kinematic
NS05	500573	4181048	2656		♦	♦	♦	kinematic
NS06	500461	4180450	2767		♦	♦	♦	kinematic
NS07	500609	4180035	2849		♦	♦	♦	kinematic
NS08	500187	4179784	2936		♦	♦	♦	kinematic
NS09	499284	4179618	3006		♦	♦	♦	kinematic
NS10	498946	4179351	3024		♦	♦	♦	kinematic
NS11	498964	4178737	3140		♦	♦	♦	kinematic
NS12	498849	4178351	3142		♦	♦		kinematic
NS13	498656	4177738	3051		♦	♦		kinematic
NS14	498999	4177187	3021		♦	♦		kinematic
NS15	499653	4176832	2984		♦	♦		kinematic
NS16	499984	4176345	2862		♦	♦	♦	kinematic
NS17	500041	4176114	2798		♦	♦	♦	kinematic
NS18	500386	4175473	2689		♦	♦	♦	kinematic
NS19	499959	4174704	2553		♦	♦	♦	kinematic
NS20	499759	4174442	2476		♦	♦	♦	kinematic
NS21	499579	4173308	2175		♦	♦	♦	kinematic
NS22	500009	4172669	1973		♦	♦	♦	kinematic
NUN	495830	4179543	1830	♦	♦	♦	♦	static
OBS	501342	4180162	2819	♦	♦	♦	♦	static
OSV	501476	4179830	2867	♦	♦	♦	♦	static
PAR	497201	4170245	1552		♦	♦	♦	static
PDG	488867	4177328	1214		♦	♦	♦	static
PLU	499117	4179835	2970	♦	♦	♦	♦	static
ROC	500461	4200341	959	♦	♦	♦	♦	static
STP	505486	4172033	1328	♦	♦	♦	♦	static
TDF	500084	4176702	2966		♦	♦	♦	static
TUR	490507	4174001	1326	♦	♦	♦	♦	static

Table 2 - InSAR orbit pairs formed and relevant parameters.

ID	Image Pair	Frame	Time Span	_I_ Baseline	II Baseline	Figure
I01	1993.10.17 - 1997.05.28	747	1319 days	19 m	90 m	3b
I02	1993.11.21 - 1997.03.19	747	1214 days	-80 m	25 m	3c
I03	1993.11.21 - 1997.09.10	747	1389 days	-2 m	96 m	3d
I04	1993.11.21 - 2000.10.04	747	2509 days	-40 m	-23 m	6b
I05	1997.03.19 - 1997.09.10	747	175 days	78 m	71 m	4b
I06	1997.05.28 - 1998.05.13	747	350 days	-80 m	-33 m	4c
I07	1998.05.20 - 2000.11.15	2853	910 days	10 m	-144 m	5b
I08	1998.09.02 - 2000.10.11	2853	770 days	20 m	-42 m	5c

September to December 2000, relatively mild Strombolian activity occurred at the BNC (Fig. 2a). In late November 2000, activity resumed at the SEC producing lava flows; after a few days the activity ceased without having evolved into a new paroxysm (Behncke and Neri, 2003).

4. Data processing and methodology

We applied an integrated InSAR-GPS approach in order to analyse and investigate ground deformation patterns affecting Mt. Etna volcano during the period 1993-2000.

As a first step, data collected from GPS surveys, between 1993 and 2000 were processed. In particular, in order to allow the integration between GPS and InSAR results, comparisons of the 1993, 1997, 1998 and 2000 surveys were analysed (Fig. 2b). GPS data from each survey were processed using the Trimble Geomatics Office software. Antenna calibration models and precise ephemeredes both produced by the IGS were introduced into the processing. While for the 1993 survey here we refer to the Puglisi *et al.* (2001) solution, the three other surveys were re-processed (1997 and 1998 surveys) or processed for the first time (2000 survey) following the criteria usually adopted for the Mt. Etna GPS network (Bonforte and Puglisi, 2003). The baseline solutions resulting from each survey processing were adjusted, initially by fixing the network to its centroid, and finally by fixing an appropriate set of coordinates for the reference frame (in our case, the network was fixed to the coordinates of IIV, CES and ROC benchmarks). Table 1 shows some details for each GPS survey. The horizontal and vertical displacements of each benchmark were then estimated: i) by comparing the results of the adjustment for the 1997-1998 and 1998-2000 comparisons and ii) by combining different solutions for the 1993-1997 and 1993-2000 comparisons. The results of each GPS comparisons are reported in terms of displacement vectors and vertical motions of each GPS benchmark.

As a second step, the radar images over Mt. Etna were selected by inspecting the ERS archives by using the DESCW software. The radar images were chosen on the grounds of the two following criteria: i) to obtain image pairs having the minimum perpendicular baseline component available (to minimize temporal decorrelation) and ii) to obtain orbit pairs in order to study the same period investigated by GPS techniques (Fig. 2c). Table 2 lists the interferometric orbit pairs of radar data. The selected image pairs of data were processed by using the Atlantis EvInSAR software. The procedure used for the generation of interferometric products relevant to

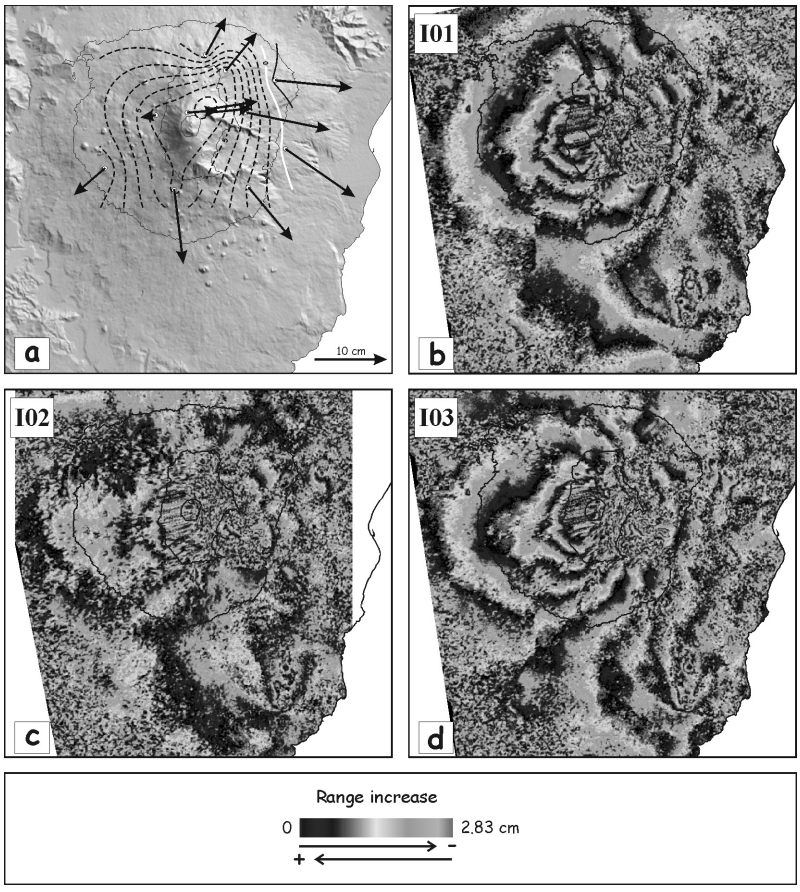

Fig. 3 - Displacement vectors and height variations from 1993 to 1997 (a). Dotted contour lines indicate uplift and solid lowering; the white line corresponds to no vertical displacement; contour interval is 1 cm. Interferograms for various time periods between 1993 - 1997: 1993.10.17 - 1997.05.28 (b); 1993.11.21 - 1997.03.19 (c) 1993.11.21 - 1997.09.10 (d). Each fringe represents a change in phase corresponding to about 2.8 cm of LOS.

the selected image pairs is the "two-pass interferometry" (Massonnet and Feigl, 1998). A photogrammetric DEM (accuracy of 10 m) and accurate orbital parameters calculated by DEOS (Delft Orbits) were introduced into the processing.

As a final step, ground deformation data were inverted assuming simple dislocations (Okada, 1985) and/or point sources of pressure change (Mogi, 1958) by adopting either a least-square (LS) method (Tarantola and Vallette, 1982) or a simplex algorithm (Nunnari *et al.,* 1995). These strategies are normally adopted to invert a relatively low number of geodetic data. The introduction of InSAR data changes not only the number of data to be inverted, but also their quality. Indeed, they are mono-dimensional and their quality varies widely across the interferogram. For these reasons, only GPS data were inverted, then for each modelled source, the expected ground deformation pattern was calculated on a grid covering the volcano edifice; finally, the expected ground deformation was projected along the LOS in order to compare the fringes calculated from the model with the observed ones. In this way, GPS results are used for validating the interferograms indirectly. On the other hand, the comparison of the synthetic interferogram with the observed one permits the validation (or rejection) of the modelled sources.

5. Ground deformation

Figs. 3, 4, 5 and 6 map the ground deformation patterns for four different time intervals: from 1993 to 1997 (Fig. 3), from 1997 to 1998 (Fig. 4), from 1998 to 2000 (Fig. 5) and from 1993 to 2000 (Fig. 6). In these figures, the ground deformations are mapped by using displacement vectors (resulting form the comparison between GPS surveys) and interferograms where each fringe represents 2.8 cm of variation in the LOS range. The reading of this last information it is not obvious. Positive LOS increase is associated to both a lowering and/or a horizontal distancing of the Earth's surfaces; conversely, negative LOS increase is associated both to an uplift and/or an approach of the Earth's surface. From the interferograms alone it is impossible to distinguish which component (vertical or horizontal) is prevailing. These figures lead to the following observations in time and space performed by the analysis of both GPS and InSAR results.

a) September 1993 - July 1997: the horizontal displacement vectors calculated using a GPS comparison for this time interval show a general radial pattern with respect to a centre of deformation located on the upper western flank (Fig. 3a). The eastern sector is indeed affected by a strong horizontal eastward displacement, with respect to the western and summit sectors. Concerning the vertical displacement, there was a general uplift of the whole edifice with a maximum of 8 cm located on the northern part of the summit area (Fig. 3a). The InSAR data (Figs. 3b, 3c, 3d) show a diffuse negative LOS variation with a roughly concentric pattern, although the comparison between I01, I02 and I03 interferograms suggests that the deformation rate was not constant throughout this interval. The I02 interferogram, indeed, measures smaller deformation than the I03 one. Considering that both I02 and I03 interferograms began in November 1993 but respectively end in March and September 1997, it is evident that the deformation increased from March to September 1997. Furthermore, because I01 and I03 interferograms have a similar deformation pattern, although they did not begin and end at the same time (Fig. 2), it is possible to conclude that the increase in the uplift rate occurred during the March-May 1997 time interval (the only period not in common between the two I01 and I02 interferograms but included in I03).
b) July 1997 - July 1998: for this period the vertical displacements measured at the network's benchmarks show a general uplift of the whole edifice (Fig. 4a). The largest vertical displacement was detected along the summit benchmarks, ranging from 3 cm to 9 cm. The western flank of the volcano is affected by a strong horizontal component of motion SW-ward trending. The eastern flank shows a lesser motion (about 1-2 cm), trending ESE in the northern part and to south in the southern part. The horizontal deformation ranges from 0.5 cm to 5 cm. The I05 (Fig. 4b) and I06 (Fig. 4c) interferograms, relevant to this time interval, show similar deformation patterns with a marked negative variation centred slightly westwards with respect to the summit craters and roughly elliptically shaped, with an elongation trending NNE-SSW. The I05 interferogram shows a larger deformed area with respect to the I06 one, interpreted as the effect of a deep source. The evidence of a deep source is lost in the I06 interferogram, whereas fringes close to the summit area here evidence a shallow source. This confirms the activation of a deep source during March-May 1997 and constrains the presence of a shallow active source between May 1997 and May 1998.
c) July 1998 - July 2000: in this time interval, GPS data put in evidence that the volcano edifice was affected by a strong subsidence, up to -10 cm on the summit and NE Rift areas (Fig. 5a).

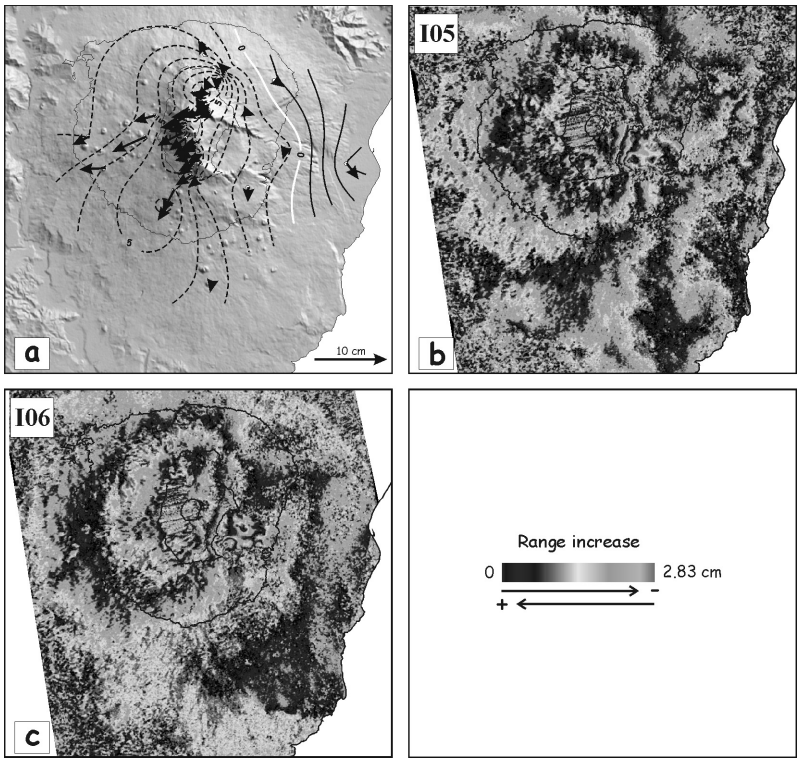

Fig. 4 - Displacement vectors and height variations from 1997 to 1998 (a). Dotted contour lines indicate uplift and solid lowering; the white line corresponds to no vertical displacement; contour interval is 1 cm. Interferograms for various time periods between 1997 - 1998: 1997.03.19 - 1997.09.10 (b); 1997.05.28 - 1998.05.13 (c).

Furthermore, the horizontal displacements indicate that the volcano is generally expanding, mainly to the east, west and south. In the I07 and I08 interferograms (Fig. 5b and 5c), more than one fringe can be recognized, suggesting a deflation of about 5-6 cm of the volcano. Although large parts of this interferogram have very low coherency values (white areas in Fig. 5b and 5c), the deflated area seems to include the summit area and the higher western and northern flanks of the volcano.

d) September 1993 - July 2000: the horizontal displacements (Fig. 6a) show a general radial pattern of the motion, with respect to a centre of deformation located on the upper western flank, as just observed for the 1993-1997 period. Regarding the vertical displacement, a general uplift of the whole edifice with a maximum of 10 cm located on the upper southern flank is observed. Concerning the InSAR data, the deformation patterns (Fig. 6b) show a general line of sight (LOS) negative variation, having a similar shape to that observed for the 1993-1997 period, but presenting a higher number of concentric fringes, as expected due to the longer time span covered. The fringes are centred on the upper western flank of the volcano edifice, accounting for more than 14 cm of shortening in the LOS satellite direction.

6. Data inversion

As above mentioned, the observed ground deformation derived from GPS data were inverted

Table 3 - Parameters of the modelled sources for all the GPS comparisons considered in this work. Coordinates are in UTM projection.

1993 - 1997				
Parameters	**Plane of sliding**			**Point source**
Longitude (km)	504.200			496.96
Latitude (km)	4172.030			4179.45
Azimuth	N21°E			
Depth (km)	1.4 b.s.l.			6.78 b.s.l.
Length (km)	26.4			
Width (km)	12.34			
Dip	11.6°			
Strike-slip (cm)	-4.4 ± 0.3			
Dip-slip (cm)	16.1 ± 0.4			
Opening (cm)	0			
$P*a^3$ ($Pa*m^3$)				4.12E+17

1997 - 1998				
Parameters	**Plane of sliding**	**Dyke**	**NE source**	
Longitude (km)	504.20	500.70 ± 0.02	502.30 ± 0.02	
Latitude (km)	4172.03	4178.50 ± 0.02	4182.80 ± 0.01	
Azimuth	N21°E	N158°E ± 0.5	N163°W ± 0.5	
Depth (km)	1.4 b.s.l.	1.05 ± 0.4 a.s.l.	0.88 ± 0.06 a.s.l.	
Length (km)	26.4	8.76 ± 0.05	6.0 ± 0.05	
Width (km)	12.34	5.5 ± 0.06	3.40 ± 0.05	
Dip	11.6°	53.1° ± 0.7	46° ± 1.0	
Strike-slip (cm)	-2.7 ± 0.1	0	-2.0 ± 0.1	
Dip-slip (cm)	1.3 ± 0.1	0	-1.0 ± 0.1	
Opening (cm)	0	13.7 ± 0.2	10.1 ± 0.1	

1998 - 2000				
Parameters	**Plane of sliding**	**S source**	**NE source**	
Longitude (km)	504.20	499.70 ± 0.01	500.90 ± 0.01	
Latitude (km)	4172.03	4175.66 ± 0.01	4181.95 ± 0.01	
Azimuth	N21°E	N14°W ± 0.4	N39°E ± 0.3	
Depth (km)	1.40 b.s.l.	0.4 ± 0.01 a.s.l.	1.8 ± 0.01 a.s.l.	
Length (km)	26.40	3.14 ± 0.02	8.40 ± 0.03	
Width (km)	12.34	3.37 ± 0.03	2.50 ± 0.03	
Dip	11.6°	49.3° ± 0.4	39° ± 0.4	
Strike-slip (cm)	-3.6 ± 0.2	3.2 ± 0.2	-2.07 ± 0.1	
Dip-slip (cm)	9.6 ± 0.2	25.6 ± 0.2	16.4 ± 0.1	
Opening (cm)	0	0	1.1 ± 0.1	

1993 - 2000				
	Plane of sliding			**Point source**
Longitude (km)	504.20			496.931
Latitude (km)	4172.03			4181.336
Azimuth	N21°E			
Depth (km)	1.4 b.s.l.			8.1 b.s.l.
Length (km)	26.40			
Width (km)	12.34			
Dip	11.6°			
Strike-slip (cm)	-9.6 ± 0.2			
Dip-slip (cm)	26.1 ± 0.2			
Opening (cm)	0			
$P*a^3$ ($Pa*m^3$)				6.89E+17

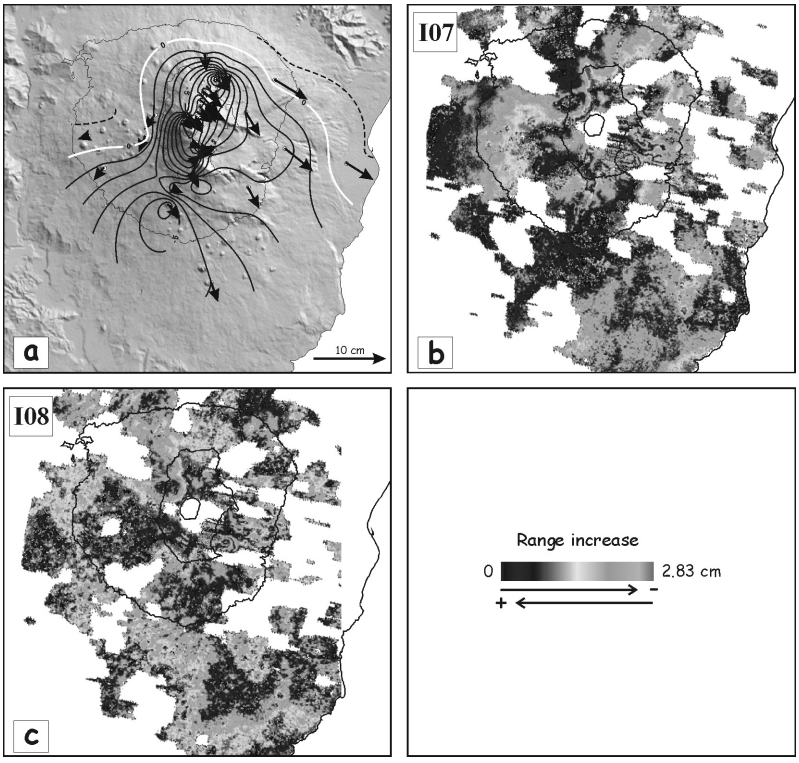

Fig. 5 - Displacement vectors and height variations from 1998 to 2000 (a). Dotted contour lines indicate uplift and solid lowering; the white line corresponds to no vertical displacement; contour interval is 1 cm. Interferograms for various time periods between 1998 - 2000: 1998.05.20 - 2000.11.15 (b); 1998.09.02 - 2000.10.11 (c).

assuming simple dislocations (Okada, 1985) and/or point sources of pressure change (Mogi, 1958) in an elastic half-space, by adopting a LS method or the simplex algorithm. In this step, both horizontal and vertical GPS components were inverted by taking into account the experimental errors. Values of 30 GPa and 0.25 respectively for the shear modulus and Poisson's ratio were assumed in the inversion. The rigidity chosen represents an averaged value for crustal rigidity of Mt. Etna (e.g. Williams and Wadge, 2000; Trasatti *et al.,* 2003; Puglisi and Bonforte, 2004).

6.1. 1993 - 1997 data inversion

The simplex algorithm [for details see Nunnari *et al.,* (1995)] was adopted to invert this data set assuming the Mogi (1958) formalism. The parameter space has been sampled by running several minimum function searches, each search starting from a different set of parameter values. All the solutions of the searches converged to a unique pressure source located beneath the upper western flank of the volcano (Fig. 7a), at a depth of 6.8 km b.s.l., with a strength of $4.17 \cdot 10^{17}$ Pa·m^3. Since the benchmarks are affected by larger residuals on the eastern flank, a further inversion by using an LS approach was performed, starting from the source obtained from the simplex inversion and introducing a sub-horizontal source (hereafter plane of sliding), lying beneath the eastern flank, defined in Palano (2003) into the computation. The positions and dimensions of the plane of sliding were kept fixed, inverting only its dip- and strike-motion (its opening was forced to zero). The combination of the two sources (Fig. 7a) significantly improved

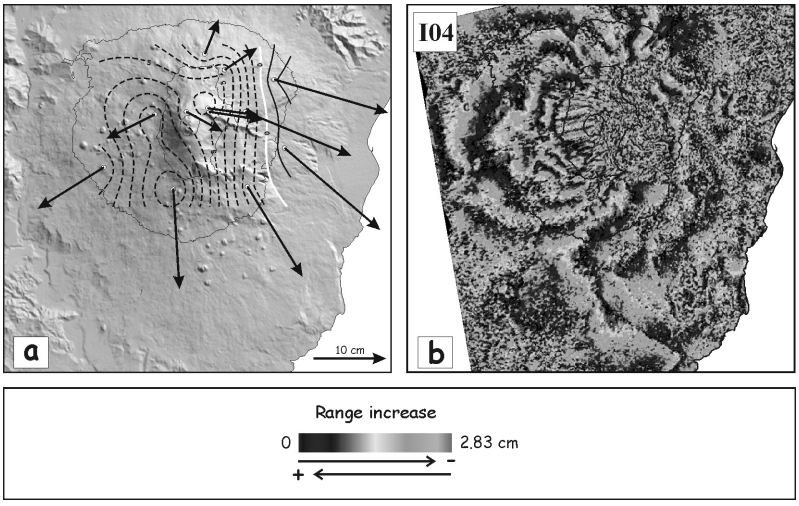

Fig. 6 - Displacement vectors and height variations from 1993 to 2000 (a). Dotted contour lines indicate uplift and solid lowering; the white line corresponds to no vertical displacement; contour interval is 1 cm. Interferograms for the 1993.11.21 - 2000.10.04 time interval (b).

the fit of data over the entire area. The results of this inversion are summarized in Table 3. The synthetic interferogram is reported in Fig. 7b; it can be compared with interferograms I01 and I03.

6.2. 1997 - 1998 data inversion

This GPS data set was previously processed using both different processing software and different sets of coordinates for the reference system in Puglisi and Bonforte (2004). The ground deformation pattern resulting from the comparison has a similar shape and only a substantial difference regarding the height change is noteworthy. Three sources were detected: a dike located on the north-western flank of the volcano at 0.7 km a.s.l. and two sliding surfaces located under the southern and eastern flank, respectively deep 0.5 km a.s.l. and 1.7 km b.s.l. (Puglisi and Bonforte, 2004). Starting from this model, several inversions were performed by using an LS approach, in order to refine the dike parameters to fit GPS data. Unfortunately, the source proposed by Puglisi and Bonforte (2004) is not able to fit the entire ground deformation, especially on the NE Rift area and on the eastern flank. For this reason, a further inversion was performed, starting from results of the last one and introducing another two dislocations into the computation. The former is the plane of sliding, just defined in the previous section, while the latter is a vertical dislocation plane located beneath the NE Rift area. In this case too, the position and dimension of the plane of sliding were kept fixed, inverting only its dip- and strike-motion (its opening was forced to zero). The combination of those three sources (Fig. 7c) significantly improved the fit to the data, except for some benchmarks, probably affected by local effects. The results of this inversion are summarized in Table 3. The synthetic interferogram reported in Fig. 7d can be compared with interferogram I06 (Fig. 4c).

6.3. 1998 - 2000 data inversion

This inversion was performed using the simplex algorithm and assuming the Okada (1985) model. As a starting point we used the vertical dislocation plane used for the previous inversion. The best solution converged to a shallow plane located beneath the NE Rift, striking NE-SW and

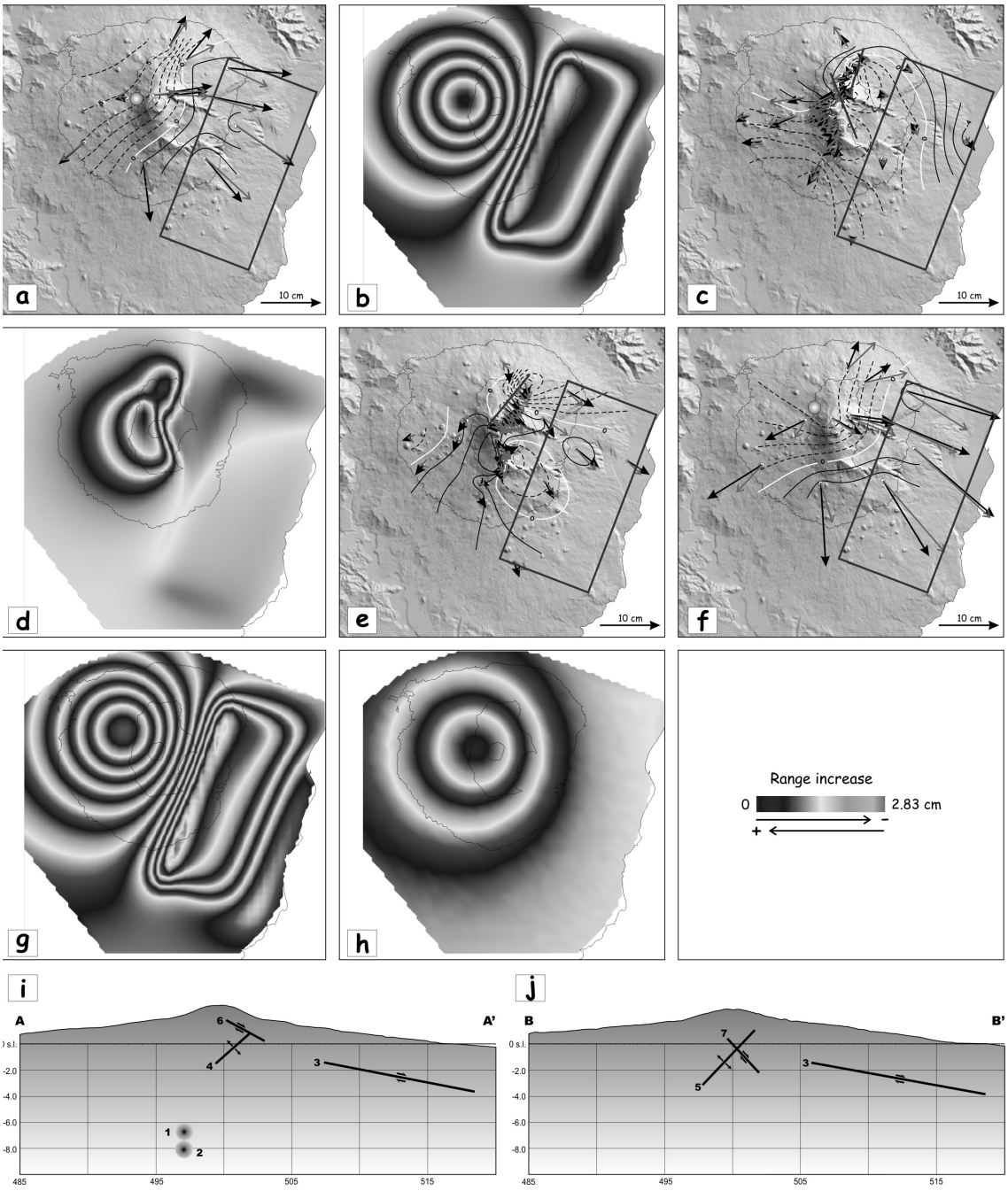

Fig. 7 - GPS data inversions (a, c, e, f) and relevant synthetic interferograms (b, d, g): a) 1993-1997 data inversions; c) 1997-1998 data inversions; e) 1998-2000 data inversions; f) 1993-2000 data inversions. Comparison between observed and calculated displacements; modelled sources are also reported. Observed horizontal vectors are in black; calculated horizontal vectors in grey. Contours define the final residual between observed and calculated vertical displacements; dotted line for positive values, solid line for negative; the contour interval is 1 cm. h) synthetic interferogram calculated from pressure source for the 1996-1997 period as proposed by Puglisi and Bonforte (2004). i) and j) schematic cross sections (A-A', B-B') showing the geometrical relationships between the different structures modelled in this work (see Table 3): 1) 1993-1997 point source; 2) 1993-2000 point source; 3) plane of sliding; 4) 1997-1998 dike; 5) 1997-1998 NE source; 6) 1998-2000 NE source; 7) 1998-2000 S source.

dipping to SE. However, this source was unable to fit the ground deformation over the entire area, so a new inversion was performed. The "NE source" was constrained to the values resulting from the previous inversion, and a new vertical plane located on the S Rift area was introduced into the computation. The plane of sliding was also introduced into the computation by adopting the same approach used in the previous inversion. Finally, the results of the inversion were able to fit the ground deformation over the entire area (Fig. 7e). The results of this inversion are summarized in Table 3. Due to the low quality of the interferograms for this period, no synthetic data from models was calculated for the comparison.

6.4. 1993 - 2000 data inversion

This time interval covers the entire period analysed in this work. In order to maintain the same structural framework (i.e. point source + plane of sliding source) the inversion was performed adopting the same strategy used for 1993-1997 time interval. Obviously this approach produces sources representing an average of those previously obtained for the different time intervals.

The best solution is given by a pressure source located beneath the upper western flank of the volcano (Fig. 7f), at a depth of about 8.1 km, with a strength of $6.9 \cdot 10^{17}$ Pa·m^3, while the plane of sliding showed a slip dominated by a normal dip-slip component. Table 3 summarizes the results of this inversion. The synthetic interferogram reported in Fig. 7g can be compared with interferogram I04.

7. Discussion

Mt. Etna GPS and InSAR analyses between 1993 and 1997, indicate a re-pressurization of the plumbing system which i) triggered most of the seismicity, ii) induced the dilatation of the volcano and iii) produced a series of summit eruptions since 1995.

InSAR data between March and May 1997, detected a deep intrusion centred beneath the western flank of the volcano. Puglisi and Bonforte (2004) suggested that a deep source was recharging from July 1996 - July 1997. By inverting GPS data, they indeed inferred a pressure source located beneath the western flank of the volcano at 9 km b.s.l. (Puglisi and Bonforte, 2004). The synthetic interferogram (Fig. 7h) calculated from the expected deformation pattern of this source, shows a good agreement with interferogram I05 (Fig. 4b).

In the months following, this intrusion seems to rise up leading to a seismic swarm occurring between January 9 - 14, 1998 in the western sector (Bonaccorso and Patanè, 2001). The shallow intrusion is also confirmed by GPS data, by comparing the 1997 and the surveys 1998. After the summer of 1998, GPS and InSAR data detected a general deflation up to 2000 affecting the upper part of the volcano. A more precise timing of this phenomenon is impossible with the considered data set.

The inversions of GPS data for long-time periods (1993 - 1997 and 1993 - 2000) propose the presence of pressure sources beneath the upper western flank of the volcano, at 7-8 km b.s.l.. However, these pressure sources could be interpreted as a sort of average of the sources that were active throughout the seven-year period. Several papers have analyzed and modelled ground deformation, at different time intervals, after the 1991-1993 Mt. Etna eruption, using data collected both by geodetic (Puglisi *et al.,* 2001; Bonforte and Puglisi, 2003) and by InSAR

techniques (Lanari *et al.,* 1998; Lundgren *et al.,* 2003, 2004) that show the presence of active ground deformation sources at depths ranging from 3 to 9 km b.s.l. beneath the upper western flank of Mt. Etna and active at different times. These results could be related both to the uncertainties of the different techniques used for measuring and inverting the deformation data and/or to the actual movement of the magma in the plumbing system. Considering the results of this study, we suggest that at least a part of the feeding system of Mt. Etna is centred beneath the upper western part of the volcano, located in a volume whose projection on the surface is relatively small (few km^2). This conclusion is confirmed by a recent seismic tomography of the crustal structure of Mt. Etna (Laigle *et al.,* 2000; Patanè *et al.,* 2002).

The combination of the structures inferred from the 1997 - 1998 and 1998 - 2000 inversions locally forms two graben-like structures located beneath the NE and S Rift areas. The two graben-like structures, characterized by low-dip-angle planes, trending NNW-SSE and NE-SW, represent the main orientation of the magmatic intrusions and tensile dislocations at Mt. Etna. These two primary structural trends are easily recognizable in the structural framework of the area (Fig. 1). Furthermore, seismicity often takes place in swarms and/or clusters along those principal structural trends at Mt. Etna (Laigle *et al.,* 2000; Patanè *et al.,* 2002).

GPS and InSAR data also evidenced a constant eastward to south-eastward movement of the eastern flank of the volcano. This movement represents an important feature of the volcano dynamics, as highlighted by several points of view (geological, structural, geophysical) from different studies (e.g., Kieffer, 1985; Borgia *et al.,* 1992; Rust and Neri, 1996; Froger *et al.,* 2001; Bonforte and Puglisi, 2003). In this paper, using the Okada (1985) formalism using the best fitting model is given by a plane dipping about 12° ESE and located beneath the eastern flank of the volcano, 1.4 km b.s.l. deep. Although the Okada (1985) formalism seems to be an approximation to model a ground deformation pattern produced by a sliding source, it has been successfully applied in Hawaii (e.g. Owen *et al.,* 2000; Cervelli *et al.,* 2002) to perform a first-order modelling of the deformation pattern in similar conditions. This plane drives the south-eastward motion of a sector bounded to the north by the Pernicana fault, to the west by the NE Rift and the south Rift, and to the south by the Mascalucia-Tremestieri-Trecastagni fault system. This structural framework leads to the interpretation of the eastern sector of the volcano as a mega-block bounded by shallow trans-tensional faults, which progressively flatten at a depth (1-2 km b.s.l.) into a main zone which is described by the plane of sliding in the analytical model. In the investigated period, the mega-block moved towards the Ionian Sea with an average slip-rate of about 2.4 cm/y.

8. Concluding remarks

Ground deformation at Mt. Etna has been studied using both ERS-1/2 SAR and GPS data. The integrated InSAR-GPS approach applied in this paper allowed us to investigate highly accurate deformations (i.e. at sub-centimetre levels) with unprecedented spatial coverage affecting a large volcanic area such as Mt. Etna. Both the techniques highlight some features of the volcano's behaviour from 1993 to 2000. By looking at different ground deformation patterns during different time windows we can draw the following conclusions.

1. InSAR and GPS data show that from 1993 the magma has started to fill the plumbing system of the volcano. However only in 1995 did the summit eruptions begin. InSAR data fix the timing of the deep source, active between July 1996 and July 1997, inferred by Puglisi and Bonforte (2004). In this study, the effect of a deep intrusion on the western flank of the volcano, between March and May 1997, compatible with that found in a previous study, was indeed detected. In the following months this intrusion rose up leading to a seismic swarm in January 1998. From 1998 to 2000, a general deflation affected the upper part of the volcano.
2. Elastic deformation modelling of the GPS data suggests that the active sources of deformation in the investigated period include deep pressure sources located beneath the upper western flank of the volcano at 7-8 km b.s.l. and shallow dislocation sources (1-2 km a.s.l) located beneath the NE and S Rift zone.
3. Both GPS and InSAR data showed a continuous eastward to south-eastward motion of part of the eastern sector of the volcano. Data confirm the boundaries of the sliding sector: the Pernicana fault to the north, the NE Rift and the S Rift to the west and the Mascalucia-Tremestieri-Trecastagni fault system to the south. The bottom of this sector was modelled by a plane dipping about 12° ESE, located beneath the eastern flank of the volcano at a depth of 1.5 km b.s.l..

Acknowledgments. We are grateful to Alessandro Caporali and an anonymous reviewer for their suggestions and for their fruitful comments on the paper. M. Palano was supported by University of Catania PhD grants.

REFERENCES

Azzaro R.; 1999: *Earthquake surface faulting at Mt. Etna volcano (Sicily) and implications for active tectonics*. J. Geodynamics, **28**, 193-213.

Behncke B. and Neri M.; 2003: *The July-August 2001 eruption of Mt. Etna (Sicily)*. Bull. Volcanol., **65**, 461-476.

Bonaccorso A. and Patanè D.; 2001: *Shear response to an intrusive episode at Mt. Etna volcano (January 1998) inferred through seismic and tilt data*. Tectonophysics, **334**, 61-75.

Bonforte A. and Puglisi G.; 2003: *Magma uprising and flank dynamics on Mount Etna volcano studied using GPS data (1994-1995)*. J. Geophys. Res., **108**, 2153-2162.

Borgia A., Ferrari L. and Pasquarè G.; 1992: *Importance of gravitational spreading in the tectonic and volcanic evolution of Mount Etna*. Nature, **357**, 231-235.

Bousquet J.C. and Lanzafame G.; 2004: *The tectonics and geodynamics of Mt. Etna: synthesis and interpretation of geological and geophysical data*. In: Bonaccorso A., Calvari S., Coltelli M., Del Negro C. and Falsaperla S. (eds), Etna Volcano Laboratory, Geophys. Monogr. Ser., vol. 143, AGU, Washington, D. C., pp. 29-47.

Coltelli M., Pompilio M., Del Carlo P., Calvari S., Pannucci S. and Scribano V.; 1998: *Mt. Etna: the eruptive activity*

(1993 - 1995). Acta Vulcanologia, **10**, 141-148.

Froger J. L., Merle O., and Briole P.; 2001: *Active spreading and regional extension at Mount Etna imaged by SAR interferometry*. Earth Planet. Sci. Lett., **148**, 245-258.

Gresta S., Bella D., Musumeci C. and Carveni P.; 1997: *Some efforts on active faulting processes (earthquakes and aseismic creep) acting on the eastern flank of Mt. Etna (Sicily)*. Acta Vulcanol., **9**, 101-108.

Kieffer G.; 1985: *Evolution structurales et dynamique d'un grand volcan polygénique: stades d'édification et d'activité actuelle de l'Etna (Sicile)*. Thesis Univ. de Clermod-Ferrand, France, 497 pp.

Laigle M., Hirn A., Sapin M., Lépine J.C., Diaz J., Gallart J. and Nicolich R.; 2000: *Mount Etna dense array local earthquake P and S tomography and implications for volcanic plumbing*. J. Geophys. Res., **105**, 21633-21646.

Lanari R., Lundgren P. and Sansosti E.; 1998: *Dynamic deformation of Etna volcano observed by satellite radar interferometry*. Geophys. Res. Lett., **25**, 1541-1544.

Lo Giudice E. and Rasà R.; 1992: *Very shallow earthquakes and brittle deformations in active volcanic areas: the Etnean region as an example*. Tectonophysics, **202**, 257-268.

Lundgren P., Berardino P., Coltelli M., Fornaro G., Lanari R., Puglisi G., Sansosti E. and Tesauro M.; 2003: *Coupled magma chamber inflation and sector collapse slip observed with SAR interferometry on Mt. Etna volcano*. J. Geophys. Res., **108**, 2247-2261.

Lundgren P., Casu F., Manzo M., Pepe A., Berardino P., Sansosti E. and Lanari R.; 2004: *Gravity and magma induced spreading of Mount Etna volcano revealed by satellite radar interferometry*. Geophys. Res. Lett., **31**, doi:10.1029/2003GL018736.

Massonnet D. and Feigl K.; 1998: *Radar interferometry and its application to changes in the Earth's surface*. Rev. Geophys., **36**, 441-500.

Nunnari G., Puglisi G., Maugeri S.R.; 1995: *An optimisation approach for the inversion of the ground deformation data*. In: Proceed. of the Workshop New Challenges for Geodesy in Volcanic Monitoring Walferdange - Luxembourg June 14-16, 1993, Cahiers du Centre Européen de Géodynamique et de Séismologie, **8**, 329-348.

Mogi K.; 1958: *Relation between the eruptions of various volcanoes and the deformations of the ground surface around them*. Bull. Earth Res. Inst., **36**, 99-134.

Okada Y.; 1985: *Surface deformation due to shear and tensile fault in half-space*. Bull. Seismol. Soc. Am., **75**, 1135-1154.

Omori F.; 1914: *The Sakurajima eruptions and earthquakes*. Bulletin of the Imperial Earthquake Investigation Committee, **8**, 1-6.

Owen S., Segall P., Lisowski M., Miklius A., Denlinger R. and Sako M.; 2000: *Rapid deformation of Kilauea Volcano: Global Positioning System measurements between 1990 and 1996*. J. Geophys. Res., **105**, 18983-18998.

Palano M.; 2003: *InSar techniques in structural geology: some applications to Mt. Etna volcano*. PhD Thesis, Università degli Studi di Catania, Italy, 165 pp.

Patanè D., Chiarabba C., Cocina O., De Gori P., Moretti M. and Boschi E.; 2002: *Tomographic images and 3D earthquake locations of the seismic swarm preceding the 2001 Mt. Etna eruption: evidence for a dike intrusion*. Geophys. Res. Lett., **29**, doi:10.1029/2001GL014391.

Puglisi G. and Bonforte A.; 2004: *Dynamics of Mount Etna volcano inferred from static and kinematic GPS measurements*. J. Geophys. Res., **109**, doi:10.1029/2003JB002878.

Puglisi, G. and Guglielmino F.; 1995: *Sperimentazione del GPS semicinematico per applicazioni geodinamiche*. In: Proceedings of XIII Meeting "Gruppo Nazionale di Geofisica della Terra Solida", Roma, 28-30 November 1994, pp. 361-372.

Puglisi G., Bonforte A. and Maugeri S. R.; 2001: *Ground deformation patterns on Mt. Etna, between 1992 and 1994, inferred from GPS data*. Bull. Volcanol., **62**, 371-384.

Rasà R., Azzaro R. and Leonardi O.; 1996: *Aseismic creep on faults and flank instability at Mt. Etna volcano*. In: McGuire W. J., Jones A. P., and Neuberg J. (eds), Volcano instability on the Earth and other planets, Geol. Soc. Spec. Publ. 110, pp. 179-192.

Rothery D.A., Coltelli M., Pirie D. and Wooster M.J.; 2001: *Documenting surface magmatic activity at Mount Etna using ATSR remote sensing*. Bull. Volcanol., **63**, 387-397.

Rust D. and Neri M.; 1996: *The boundaries of large-scale collapse on the flanks of Mount Etna, Sicily*. In: McGuire W. J., Jones A. P., and Neuberg J. (eds), Volcano instability on the Earth and other planets, Geol. Soc. Spec. Publ.

110, 193-208.

Tarantola, A., and Vallette B.; 1982: *Generalized nonlinear inverse problems solved using the least squares criterion*. Rev. Geophys. Space Phys., **20**, 219-232.

Trasatti E., Giunchi C. and Bonafede M.; 2003: *Effects of topography and rheological layering on ground deformation in volcanic regions. J. Volcanol. Geotherm*. Res., **122**, 89-110.

Williams C.A. and Wadge G.; 2000: *An accurate and efficient method for including the effects of topography in three-dimensional elastic models of ground deformation with applications to radar interferometry*. J. Geophys. Res., **105**, 8103-8120.

Corresponding author: Mimmo Palano
Istituto Nazionale di Geofisica e Vulcanologia, Sezione di Catania,
P.zza Roma 2, 95123 Catania (Italy)
phone +39 95 7165809; fax +39 95 435801; e.mail: palano@ct.ingv.it